Structural Characterization of LRRK2 Inhibitors

Gilsbach, Bernd K; Messias, Ana C; Ito, Genta; Sattler, Michael; Alessi, Dario R; Wittinghofer, Alfred; Kortholt, Arjan

Published in:
Journal of Medicinal Chemistry

DOI:
10.1021/jm5018779

Publication date:
2015

Journal of Medicinal Chemistry

Article

pubs.acs.org/jmc

Structural Characterization of LRRK2 Inhibitors

Bernd K. Gilsbach,[†] Ana C. Messias,[‡,§] Genta Ito,[∥] Michael Sattler,[‡,§] Dario R. Alessi,[∥] Alfred Wittinghofer,[⊥] and Arjan Kortholt*[,†]

[†]Department of Cell Biochemistry, University of Groningen, 9747AG Groningen, The Netherlands

[‡]Institute of Structural Biology, Helmholtz Zentrum München, Ingolstädter Landstrasse 1, 85764 Neuherberg, Germany

[§]Center for Integrated Protein Science Munich at Biomolecular NMR Spectroscopy, Department Chemie, Technische Universität München, Lichtenbergstrasse 4, 85747 Garching bei München, Germany

[∥]University of Dundee, DD1 4HN Dundee, Scotland

[⊥]Max-Planck Institut für Molekulare Physiologie, 44202 Dortmund, Germany

Supporting Information

ABSTRACT: Kinase inhibition is considered to be an important therapeutic target for LRRK2 mediated Parkinson's disease (PD). Many LRRK2 kinase inhibitors have been reported but have yet to be optimized in order to qualify as drug candidates for the treatment of the disease. In order to start a structure−function analysis of such inhibitors, we mutated the active site of *Dictyostelium* Roco4 kinase to resemble LRRK2. Here, we show saturation transfer difference (STD) NMR and the first cocrystal structures of two potent in vitro inhibitors, LRRK2-IN-1 and compound **19**, with mutated Roco4. Our data demonstrate that this system can serve as an excellent tool for the structural characterization and optimization of LRRK2 inhibitors using X-ray crystallography and NMR spectroscopy.

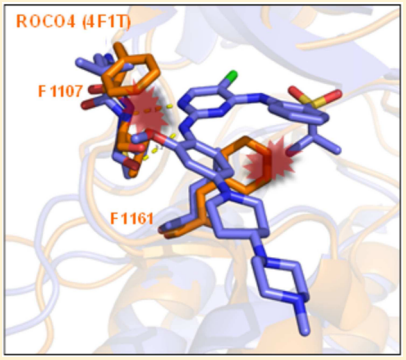

INTRODUCTION

Parkinson's disease (PD) is the second most common neurodegenerative disorder and is affecting 2% of the population above 65 years.[1] Genome-wide association screens revealed that several missense mutations in the LRRK2 gene are found in both hereditary and sporadic PD.[2−4] LRRK2 is a 286 kDa multidomain protein that belongs to the Roco family of G-proteins. LRRK2 consists of N-terminal armadillo, ankyrin, and LRR repeats followed by a small GTPase like domain called Roc (Ras of complex proteins), a COR (C-terminal of Roc), a kinase, and a WD40 domain. Mutations associated with PD have been found in nearly every domain of LRRK2, and several have been linked to increased kinase and decreased GTPase activity, suggesting a gain of function mechanism.[5] The most prevalent G2019S mutation is located in the kinase domain and leads to a 2- to 4-fold increase in kinase activity.[6−9] Therefore, the major focus of academic labs and the pharmaceutical industry has been to develop kinase inhibitors as potential therapeutics. Several LRRK2 inhibitors have been reported, but many of the them lack selectivity or the capability to pass the blood−brain barrier.[10−15] Furthermore, the recently published LRRK2 specific and brain penetrant inhibitors lead to kidney and lung abnormality.[16] Hence, though the current kinase inhibitors cannot be used for the treatment of LRRK2-mediated PD, they are being used as important tools to characterize the function and activation mechanism of LRRK2.[17−21]

Structural understanding of LRRK2 has come mainly from studies using Roco proteins from lower organisms.[22,23] Importantly, our structural studies with the *Dictyostelium* Roco4 kinase domain revealed that the increased kinase activity of LRRK2(G2019S) is caused by an additional hydrogen bond between Ser2019 (Ser1179 in Roco4) and residue Gln1918 (Arg1077 in Roco4) coming from the αC-helix, which stabilizes the active kinase conformation.[23]

In this study, we generated mutants of *Dictyostelium* Roco4 kinase such that its active site resembles more human LRRK2 kinase. Subsequently, these Roco4 mutants were used together with the wild type kinase as tools to biochemically and structurally characterize LRRK2 specific inhibitors at a molecular level.

RESULTS

Designing and Characterization of Humanized Roco4.

Our previously identified structure of the Roco4 kinase in complex with the rather unspecific LRRK2 inhibitor H1152 showed that *Dictyostelium* Roco4 kinase can be used as an important tool to biochemically and structurally characterize the LRRK2 kinase, its mutations, and possibly binding of inhibitors.[23] However, all attempts to crystallize more specific LRRK2 inhibitors failed: cocrystallization of Roco4 kinase with

Received: December 4, 2014
Published: April 21, 2015

DOI: 10.1021/jm5018779
J. Med. Chem. 2015, 58, 3751−3756

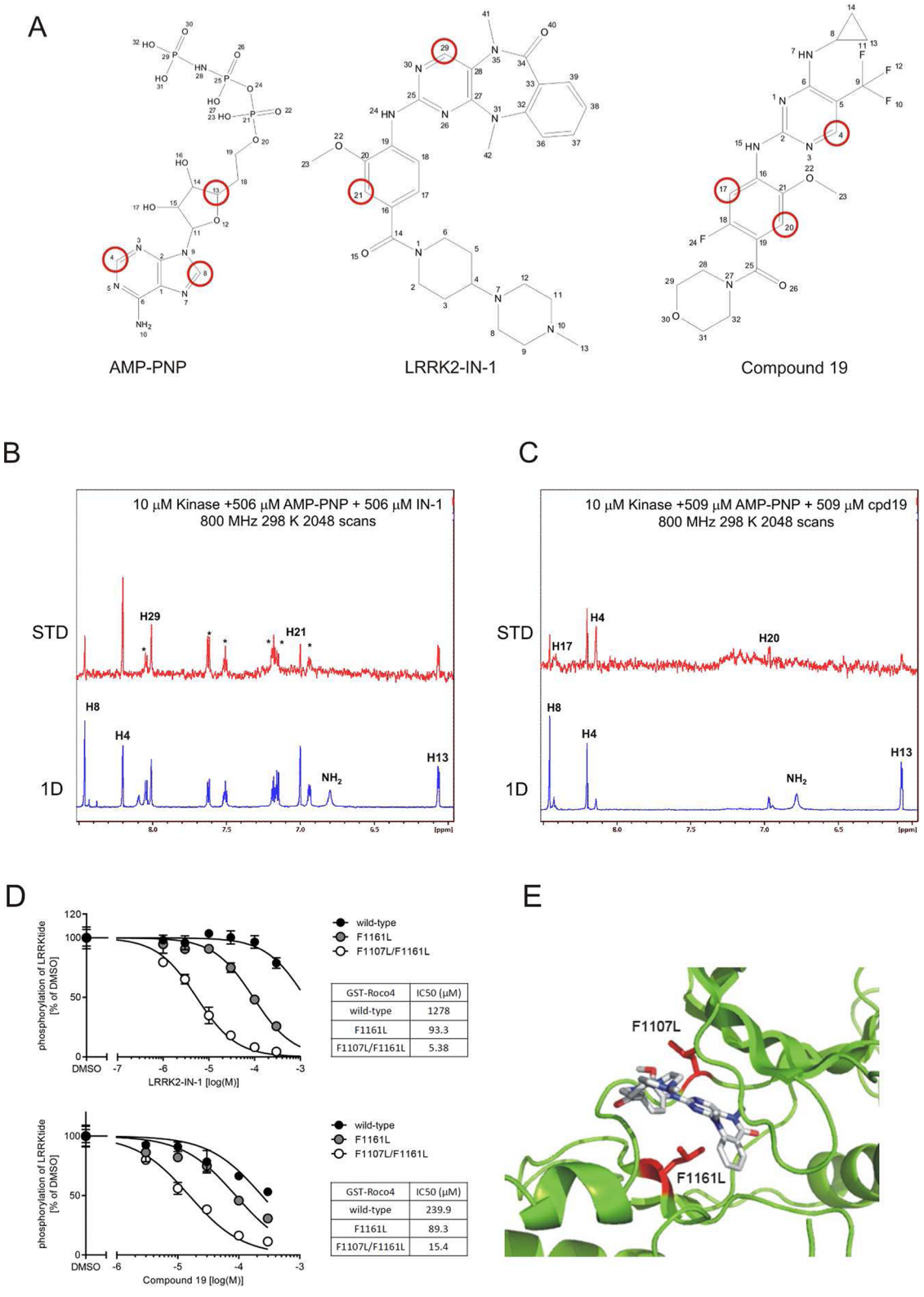

Figure 1. STD NMR and IC_{50} measurement. (A) Chemical structures of AMP-PNP, LRRK2-IN-1, and compound **19**. Proton signals observed by STD experiments are indicated by red circles. (B) STD signals from LRRK2-IN-1 and AMP-PNP protons indicate binding of both LRRK2-IN-1 and AMP-PNP to Roco4 kinase. In the 1D spectrum (blue) protons from AMP-PNP are indicated, while in the STD spectrum (red) the protons H29 and H21 from LRRK2-IN-1 are indicated. The stars denote all the aromatic protons of IN-1 for which STD signals are seen. (C) STD signals from compound **19** and AMP-PNP protons indicate binding of both compound **19** and AMP-PNP to Roco4 kinase. In the 1D spectrum (blue) protons from AMP-PNP are indicated, while in the STD spectrum (red) the pyrimidine proton H4 and the phenyl protons H17 and H20 from compound **19** are indicated. (D) IC_{50} measurement with increasing concentration of LRRK2-IN-1 and compound **19**. (E) Detailed view of the LRRK2-IN-1 bound to the humanized Roco4 kinase. The two mutated F to L are indicated in red.

DOI: 10.1021/jm5018779
J. Med. Chem. 2015, 58, 3751−3756

LRRK2-IN-1 and compound **19** led to apo crystal structures. This suggests that Roco4 has a much lower affinity for these inhibitors compared to LRRK2. We therefore analyzed inhibitor binding to Roco4 kinase with saturation transfer difference (STD) NMR,[24,25,27,28] which can detect binding of small ligands to macromolecules with dissociation constants K_D ranging from nM to mM. STD NMR is based on the transfer of saturation of magnetization from the protein to the bound ligand(s), which by exchange is then detected with the NMR signals of the free ligand. A subtraction of this spectrum from a spectrum without saturation of the protein reveals the NMR signals of ligands that are in contact with the protein. Ligand protons closer to the protein in the binding interface show the most intense STD NMR signals. An extension of this method, named ATP-STD NMR, has been developed for screening of protein kinases.[26,29] ATP-STD competition experiments with equimolar concentration of ATP analog (AMP-PNP) and LRRK2-IN-1 or compound **19** showed that both inhibitors compete with AMP-PNP for the Roco4 ATP-binding pocket (Figure 1A–C). This shows that LRRK2-IN-1 and compound **19** are both able to bind to Roco4. However, competition of these inhibitors with AMP-PNP shows signals from both AMP-PNP and the inhibitors simultaneously, indicating that the affinity of the inhibitors and thus the IC_{50} to wild type Roco4 kinase must be low, considering that ATP typically binds to kinases with a K_D of 10–100 μM. Consistent with this observation, kinase activity assays showed that LRRK2-IN-1 and compound **19** inhibit wild type Roco4 kinase with an IC_{50} of 1278 and 240 μM, respectively (Figure 1D).

Although the anticipated binding pocket of LRRK2 inhibitors in the ATP binding site is reasonably well conserved between Roco4 and LRRK2 (alignment Figure S1), modeling of one of the LRRK2 specific inhibitors (LRRK2-IN-1) into the binding pocket revealed that the Phe1107 and Phe1161 side chains of Roco4, corresponding to LRRK2 Leu1949 and Leu2001, would clash with the inhibitor upon binding (Figure 1E). Therefore, we generated Roco4 mutants, in which one or both phenylalanine was mutated to leucine. Introducing these mutations did not affect the kinase activity of the protein (V_{max}, K_m(ATP)) but led to a decrease of the IC_{50} values for LRRK2-IN-1 and compound **19**: the IC_{50} for LRRK2-IN-1 dropped from 1278 to 68 μM for the single mutant and to 5.3 μM for the double mutant, and for compound **19**, it dropped from 240 to 89 μM for the single mutant and to 15.4 μM for the double mutant (Figure 1D). This almost 175-fold preference of LRRK2-IN-1 and 15-fold preference of compound **19** for the double mutant Roco4(F1107L/F1161L) compared to wild type kinase makes this Roco4 mutant a very valuable tool for detailed structural and biochemical characterization of LRRK2 inhibitor binding. Since the *Dictyostelium* Roco4(F1107L/F1161L) mutant contains an active site resembling human LRRK2, from now on, we refer to it as humanized Roco4.

Structural Characterization of LRRK2-IN-1 Binding. LRRK2-IN-1 is the first identified LRRK2-specific inhibitor, which is now a common tool compound for the LRRK2 research community.[10] LRRK2-IN-1 has a 2-amino-5,11-dimethyl-5*H*-benzo[*e*]pyrimido[5,4-*b*][1,4]diazepine-6(11*H*)-one scaffold and inhibits LRRK2 with an IC_{50} value of 13 nM to the wild type protein and 6 nM to the G2019S mutation. LRRK2-IN-1 showed high selectivity against a panel of more than 470 kinases. In mice LRRK2-IN-1 leads to the dephosphorylation of LRRK2 residues Ser910 and Ser935 in the kidney but not in the brain, indicating that it is not capable of crossing the blood–brain barrier.[10]

Humanized Roco4 kinase containing the LRRK2-IN-1 inhibitor crystallized in space group $P2_12_12_1$ and diffracted up to 3.0 Å with two molecules in the asymmetric unit cell (Table S1). The density map was refined to a R_{work}/R_{free} of 0.25 and 0.30, respectively. The rmsd between the wild type and the inhibitor structure is 1.65 Å. The structure of the humanized kinase does not differ much from the wild type structure (Figure 2A). It shows the typical kinase fold with a mostly β-sheet containing N-terminal lobe and a α-helical C-terminal lobe. The cleft between these lobes forms the ATP binding pocket. Kinase inhibitors that bind in the ATP binding pocket have been classified as type 1 and type 2.[24,27] Type 1 molecules recognize specifically the active conformation, while type 2 inhibitors bind specifically to the inactive conformation, with additional interactions involving the DFG loop.[30] The major difference between the structure of active Roco4 kinase and inactive Roco4 kinase is the conformation of the activation loop: in the inactive state this loop is disordered, while in the phosphorylated state it reorients into the ordered active conformation.[25]

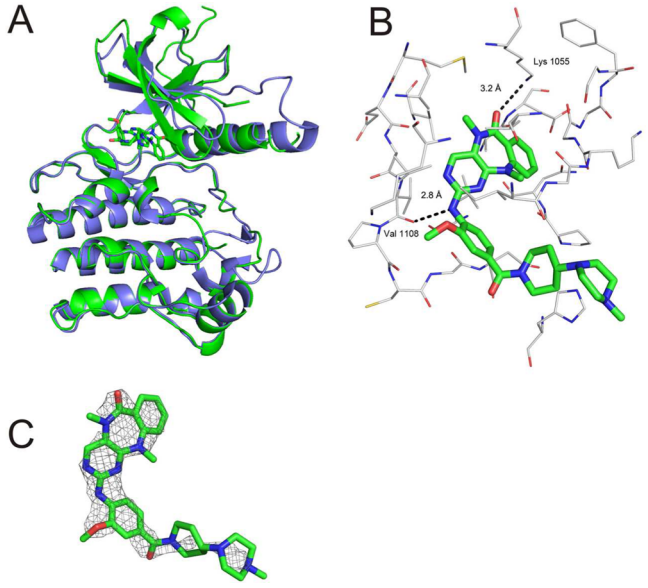

Figure 2. Cocrystal structure of Roco4 kinase and LRRK2-IN-1. (A) Overlay of the AppCp (blue) with the LRRK2-IN-1 (green) structure. (B) Close-up of the inhibitor binding pocket. Hydrogen bonds are indicated by dashed line. (C) Structure of LRRK2-IN-1. Observed electron density is indicated by mesh.

While LRRK2-IN-1 is predicted to be a type 1 inhibitor, our crystal structure suggests that it does not strictly stabilize the active conformation: the activation loop is poorly resolved indicating that it is flexible.[23] The strongest difference between the apo and LRRK2-IN-1 structures is the closure of the glycine-rich loop in the inhibitor structure. It is moved toward the C-terminal lobe by ~5 Å and covers the phosphate binding sites. The buried surface area is 530 Å^2, and the inhibitor makes 2 hydrogen bonds and 24 van der Waals contacts with the kinase. The hydrogen bonds are formed between the backbone carbonyl of Val1055 (hinge region) and the N24 of the inhibitor with a distance of 2.8 Å (3.1 Å in the other molecule) and between the Nz of Lys1055 and O40 of IN-1 with a distance of 3.2 Å (3.8 Å in the other molecule) (Figure 2B).

DOI: 10.1021/jm5018779
J. Med. Chem. 2015, 58, 3751–3756

Lys1055 is the conserved Lys from β-strand 3 (PKA:Lys72) which forms a hydrogen bond with a conserved Glu1078 (PKA:Glu91) coming from the αC-helix. The heterocyclic ring system of the LRRK2 inhibitor is accommodated by the adenine binding pocket of Roco4. The adjacent phenolic ring is partly covered by the hinge region, and the other part of the inhibitor points into the solvent. The electron density of the methyl-4-(piperidine-4-yl)piperazine moiety of the molecule is weak (Figure 2B and Figure 2C), suggesting that it is exposed to the solvent, flexible, and unlikely to contribute to binding. In NMR experiments with the wild type kinase (Figure 1A) we observe STD signals with all protons of IN-1 except the piperazine−piperidine protons (Figure S2A). Accordingly, inhibitor protons closer to the protein binding interface, i.e., the pyrimido H29 and the diazepine methyl H41 protons, which are situated between the two inhibitor−kinase hydrogen bonds mentioned above (N24(IN-1)−O(Val1055) and O40(IN-1)−Nz(Lys1055)), exhibit stronger STD signals. These observations are fully consistent with the crystal structure of the humanized kinase with IN-1.

Structural Characterization of Compound 19 Binding. Compound **19** is a type 1 inhibitor derived from a diaminopyrimidine scaffold and is able to cross the blood−brain barrier.[13] Compound **19** has an IC_{50} of 4 nM to wild type LRRK2, and when screened against a panel of 187 kinases, it only showed inhibition greater than 50% of TTK protein kinase at 0.1 μM.[12] The inhibitor compound **19** cocrystallized with the humanized kinase domain of Roco4 in space group $P4_32_12$ and diffracted to a resolution of 1.55 Å (Table S1). The density map was refined to a R_{work}/R_{free} of 0.19 and 0.21, respectively. The rmsd between the apo and the inhibitor structure is 0.97 Å. In contrast to the LRRK2-IN-1 structure, the activation loop is resolved indicating that it is less flexible and that compound **19** binds and stabilizes the active conformation. There is a slight closure of the glycine-rich loop; it is moved 2 Å toward the C-terminal lobe (Figure 3A). The inhibitor covers an area of 439 Å^2. The pyrimidine ring and the C5 trifluoromethyl and C6 aminocyclopropyl substituents cover the adenine binding pocket. The amino N15 of the inhibitor forms a hydrogen bond with the carbonyl of Val1055 of the hinge region. Furthermore, the inhibitor makes 20 van der Waals contacts. In addition to the direct contacts 2 water molecules are recognized in the crystal structure which create a hydrogen bond network between the fluorides of the inhibitor and the head groups of Asp1177 (D of the DFG motive) and Glu1078 (αC-helix) (Figure 3B). Since there are two conformations visible for Asp1177, one which is in the correct distance to the connecting water and one which is too far away (5 Å), it is likely that this interaction does not add much to the binding energy of the inhibitor. The C25 morpholino part is pointing into the solvent and has no electron density, indicated by its elevated *B*-factors, suggesting that this group is flexible and is not recognized specifically by the kinase domain (Figure 3 B and Figure 3C). In agreement with the crystal structure of the humanized kinase with compound **19** and by employment of STD NMR experiments with the wild type kinase (Figure 1B), all protons of compound **19** except the morpholino protons show STD signals (Figure S2B). Moreover, the compound protons closer to the protein binding interface show stronger STD signals, i.e., the protons closer to the hinge region (the pyrimidine H4 and the phenylmethoxy H23 and H20 protons) and the N-lobe β-strands (the cyclopropyl H13/H14 protons).

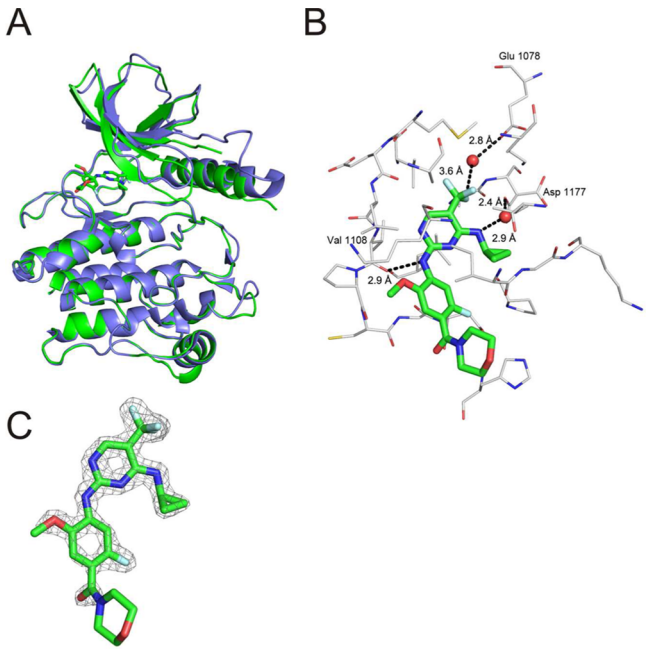

Figure 3. Cocrystal structure of Roco4 kinase and compound **19**. (A) Overlay of the AppCp (blue) with the compound **19** (green) structure. (B) Close-up of the inhibitor binding pocket. Hydrogen bonds are indicated by dashed line, and waters are shown as spheres (red). (C) Structure of compound **19**. Observed electron density is indicated by mesh.

Homology Modeling and Docking. We compared our humanized Roco4 structures with three homology models of LRRK2 that were created based on a JAK2 structure (3JY9),[13] humanized Roco4, or Roco4 in which the complete inhibitor binding pocket was mutated to that of LRRK2. Compound **19** and LRRK2-IN-1 were docked into these structures using GLIDE SP (Schroedinger Suite) with one hydrogen bond constraint to the backbone carbonyl oxygen of Val1108 (Ala1950 in the LRRK2 model).[13] All three docking models predict highly similar orientation of the inhibitors as observed in our humanized Roco4 costructures. Importantly, the long tail of the inhibitors that is not making contact with the protein in the crystal structures adopts various conformations in the docked model structures (Figure S4, parts A and B), confirming that this moiety of the inhibitors is not important for binding. Interestingly, with both inhibitors the docking scores for both Roco4 models were slightly better than for the JAK2-based LRRK2 model.

■ DISCUSSION AND CONCLUSIONS

Although the kinase domain of Roco4 and LRRK2 are quite similar (Figure S1), we were unable to cocrystallize LRRK2 specific inhibitors with Roco4 wild type, consistent with a previous study of Liu et al.[21] However, in contrast to these authors, we were able to generate Roco4 kinase mutants that efficiently bind to inhibitors. Mutation of two Phe to Leu in the catalytic site, one in the hinge region and one in β strand 6, does not change the overall fold or activity of the protein but decreased the IC_{50} values for LRRK2 inhibitors dramatically. The costructures of humanized Roco4 with both LRRK2-IN-1 and compound **19** revealed no major difference in the overall fold with the wild type AppCp Roco4 structure (Figure S3). The largest difference is the closure of the glycine-rich loop.

DOI: 10.1021/jm5018779
J. Med. Chem. 2015, 58, 3751−3756

Both compound **19** and LRRK2-IN-1 inhibit wild type and PD-related G2019S LRRK2 with similar efficiency. Consistently, the cocrystal structures reveal that Roco4 G1179 is far away from the inhibitors (approximately 11 Å) and thus cannot influence binding of the ligand. The visibility of the activation loop in the compound **19** structure indicates that this compound is clearly type 1 whereas LRRK2-IN-1 also might bind to the inactive conformation of the kinase. Both inhibitors bind in a highly similar way and make contact to the same position in the hinge region and to the conserved Lys from β3 (in the compound **19** structure mediated by a water molecule). Thus, it is rather unlikely that LRRK2 specificity is achieved by polar interactions but rather by nonpolar and van der Waals interactions. The LRRK2 DYG is only partially conserved in Roco4 (DFG) (Figure S1). However, the distance between the inhibitors and the DFG motif is approximately 10 Å, indicating that the DFG motif is not involved in the direct binding of the inhibitors. Importantly, the structures and the STD-NMR data show that the long tail of both inhibitors is not making contacts with the protein. Furthermore, the docking experiments revealed that this region of the inhibitors adopts various conformations. Altogether this suggests that the long tail of both inhibitors sticks out from the binding pocket and can thus be used for improvement of these inhibitors. Optimization of the current and identification of new LRRK2 inhibitors is urgently needed to efficiently target LRRK2-mediated. Our data show that humanized Roco4 kinase can be used as important tool in this enterprise.

EXPERIMENTAL SECTION

Purification of Humanized Roco4 Kinase and Inhibitors. Roco4 kinase (amino acids 1018−1292) was cloned into a Gateway-compatible pGEX4T1 plasmid containing an N-terminal TEV cleavage side. The two point mutations were introduced by the quick change method.[26] Proteins were purified in the presence of 1 mM ATP by GSH affinity, cleavage, and size-exclusion chromatography. The synthesis and purification of the LRRK2 inhibitors, LRRK2-IN-1, and compound **19** were previously described. The purity of both compounds is ≥95%.[10,12]

NMR Spectroscopy. NMR experiments were recorded on a 800 MHz spectrometer equipped with a TXI probe head at 298 K using 10 μM Roco4 kinase in 20 mM deuterated Tris-HCl, pH 8, 300 mM NaCl, 10 mM $MgCl_2$, 1.15 mM deuterated DTT, 0.002% NaN_3 (90% H_2O/10% D_2O). 1D proton experiments were performed using a WATERGATE pulse sequence with 32k time domain points and 64 scans. STD experiments were recorded using an interleaved pulse program with on-resonance protein irradiation at 0.75 ppm (LRRK2-IN-1) or 1.6 ppm (compound **19**) and with off-resonance irradiation at −5 ppm with 4 s total effective irradiation, using 2048 scans and 32k time domain points. Competition experiments were performed using equimolar concentrations of AMP-PNP and inhibitor: 506 μM AMP-PNP and 506 μM LRRK2-IN-1 or 509 μM AMP-PNP and 509 μM compound **19**, respectively. Spectra were processed using TOPSPIN 3.2.

IC_{50} Measurements. Roco4 kinase activity was determined at 30 °C in kinase buffer consisting of 50 mM Tris-HCl, pH 7.5, 0.1 mM EGTA, 25 μM [γ-^{32}P]ATP (~300 cpm/pmol), 10 mM $MgCl_2$, 2 mM DTT, and 150 μM LRRKtide. The reaction was started by adding Roco4 and was stopped after 5 min by spotting samples on P81 phosphocellulose papers and washing them with 50 mM phosphoric acid. The P81 papers were washed once in acetone and dried before scintillation counting. The assays were performed with 0.040 mg/mL kinase, and kinase inhibition was determined by varying the concentration of inhibitor.

Crystallography. Roco4 crystals were obtained in 100 mM 1,3-bis(tris(hydroxymethyl)methylamino)propane (pH 8,5), 200 mM Na/K tartrate, and 11% (mol/vol) PEG 3350 using the hanging drop/vapor diffusion method in the presence of 2 mM inhibitor. For data collection, crystals were cryoprotected in reservoir solution containing 20% (mol/vol) glycerol as cryoprotectant. Data sets were collected on beamline X10SA at the Swiss Light Source (Paul Scherrer Institut, Villigen, Switzerland) and were indexed, integrated, and scaled with the XDS package. Both inhibitor structures were solved by molecular replacement using the wild type Roco4 structure (PDB code 4F0G) as the search model. The model was built in COOT and refined with REFMAC5 using TLS refinement (CCP4 suite). Figures were generated using PYMOL (DeLano Scientific LLC).

Modeling and Docking. The JAK2-based model was created with the Swiss Model server, and the complete LRRK2 binding pocket was created by manually mutating the residues with Coot. Docking was performed with the docking program Glide SP.

ASSOCIATED CONTENT

Supporting Information

Crystallographic data, alignment results, NMR spectra, superposition of structures, and docking results. The Supporting Information is available free of charge on the ACS Publications website at DOI: 10.1021/jm5018779.

Accession Codes

The structure information has been deposited in the PDB under the accession codes 4YZM (Roco4 bound to LRRK2-IN-1) and 4YZN (Roco4 bound to compound **19**).

AUTHOR INFORMATION

Corresponding Author

*E-mail: A.Kortholt@rug.nl. Phone: (+31) 50-3634206.

Author Contributions

All authors contributed to the writing of the paper. B.K.G., A.W., and A.K. designed the experiments. B.K.G. performed the X-ray structural analysis, A.C.M the STD-NMR experiments, and G.I. the kinase activity measurements.

Notes

The authors declare no competing financial interest.

ACKNOWLEDGMENTS

We thank Ingrid R. Vetter for assistance with the docking experiments. This work is part of the Michael J. Fox Foundation LRRK2 Biological Structure and Function Consortium (A.K., A.W., and M.S.). A.K. is funded by an NWO-VIDI grant. Research for this project in the DRA laboratory was supported by the Michael J. Fox Foundation (award to D.R.A. and Nathanael Gray), the UK Medical Research Council, and the pharmaceutical companies supporting the Division of Signal Transduction Therapy Unit (AstraZeneca, Boehringer-Ingelheim, GlaxoSmithKline, Merck KGaA, Janssen Pharmaceutica, and Pfizer).

REFERENCES

(1) Lees, A. J.; Hardy, J.; Revesz, T. Parkinson's Disease. *Lancet* **2009**, *373*, 2055−2066.

(2) Satake, W.; Nakabayashi, Y.; Mizuta, I.; Hirota, Y.; Ito, C.; Kubo, M.; Kawaguchi, T.; Tsunoda, T.; Watanabe, M.; Takeda, A.; Tomiyama, H.; Nakashima, K.; Hasegawa, K.; Obata, F.; Yoshikawa, T.; Kawakami, H.; Sakoda, S.; Yamamoto, M.; Hattori, N.; Murata, M.; Nakamura, Y.; Toda, T. Genome-Wide Association Study Identifies Common Variants at Four Loci as Genetic Risk Factors for Parkinson's Disease. *Nat. Genet.* **2009**, *41*, 1303−1307.

(3) Zimprich, A.; Biskup, S.; Leitner, P.; Lichtner, P.; Farrer, M.; Lincoln, S.; Kachergus, J.; Hulihan, M.; Uitti, R. J.; Calne, D. B.; Stoessl, a J.; Pfeiffer, R. F.; Patenge, N.; Carbajal, I. C.; Vieregge, P.;

DOI: 10.1021/jm5018779
J. Med. Chem. 2015, 58, 3751−3756

Asmus, F.; Müller-Myhsok, B.; Dickson, D. W.; Meitinger, T.; Strom, T. M.; Wszolek, Z. K.; Gasser, T. Mutations in LRRK2 Cause Autosomal-Dominant Parkinsonism with Pleomorphic Pathology. *Neuron* **2004**, *44*, 601−607.
(4) Paisán-Ruíz, C.; Jain, S.; Evans, E. W.; Gilks, W. P.; Simón, J.; van der Brug, M.; López de Munain, A.; Aparicio, S.; Gil, A. M.; Khan, N.; Johnson, J.; Martinez, J. R.; Nicholl, D.; Carrera, I. M.; Pena, A. S.; de Silva, R.; Lees, A.; Martí-Massó, J. F.; Pérez-Tur, J.; Wood, N. W.; Singleton, A. B. Cloning of the Gene Containing Mutations That Cause PARK8-Linked Parkinson's Disease. *Neuron* **2004**, *44*, 595−600.
(5) Gilks, W. P.; Abou-Sleiman, P. M.; Gandhi, S.; Jain, S.; Singleton, A.; Lees, A. J.; Shaw, K.; Bhatia, K. P.; Bonifati, V.; Quinn, N. P.; Lynch, J.; Healy, D. G.; Holton, J. L.; Revesz, T.; Wood, N. W. Common LRRK2 Mutation in Idiopathic Parkinson's Disease. *Lancet* **2005**, *365*, 415−416.
(6) Anand, V. S.; Reichling, L. J.; Lipinski, K.; Stochaj, W.; Duan, W.; Kelleher, K.; Pungaliya, P.; Brown, E. L.; Reinhart, P. H.; Somberg, R.; Hirst, W. D.; Riddle, S. M.; Braithwaite, S. P. Investigation of Leucine-Rich Repeat Kinase 2: Enzymological Properties and Novel Assays. *FEBS J.* **2009**, *276*, 466−478.
(7) West, A. B.; Moore, D. J.; Biskup, S.; Bugayenko, A.; Smith, W. W.; Ross, C. A.; Dawson, V. L.; Dawson, T. M. Parkinson's Disease-Associated Mutations in Leucine-Rich Repeat Kinase 2 Augment Kinase Activity. *Proc. Natl. Acad. Sci. U.S.A.* **2005**, *46*, 16842−16847.
(8) Greggio, E.; Jain, S.; Kingsbury, A.; Bandopadhyay, R.; Lewis, P.; Kaganovich, A.; van der Brug, M. P.; Beilina, A.; Blackinton, J.; Thomas, K. J.; Ahmad, R.; Miller, D. W.; Kesavapany, S.; Singleton, A.; Lees, A.; Harvey, R. J.; Harvey, K.; Cookson, M. R. Kinase Activity Is Required for the Toxic Effects of Mutant LRRK2/dardarin. *Neurobiol. Dis.* **2006**, *23*, 329−341.
(9) Jaleel, M.; Nichols, R. J.; Deak, M.; Campbell, D. G.; Gillardon, F.; Knebel, A.; Alessi, D. R. LRRK2 Phosphorylates Moesin at Threonine-558: Characterization of How Parkinson's Disease Mutants Affect Kinase Activity. *Biochem. J.* **2007**, *405*, 307−317.
(10) Deng, X.; Dzamko, N.; Prescott, A.; Davies, P.; Liu, Q.; Yang, Q.; Lee, J.-D.; Patricelli, M. P.; Nomanbhoy, T. K.; Alessi, D. R.; Gray, N. S. Characterization of a Selective Inhibitor of the Parkinson's Disease Kinase LRRK2. *Nat. Chem. Biol.* **2011**, *7*, 203−205.
(11) Reith, A. D.; Bamborough, P.; Jandu, K.; Andreotti, D.; Mensah, L.; Dossang, P.; Choi, H. G.; Deng, X.; Zhang, J.; Alessi, D. R.; Gray, N. S. GSK2578215A; a Potent and Highly Selective 2-Arylmethyloxy-5-substitutent-*N*-arylbenzamide LRRK2 Kinase Inhibitor. *Bioorg. Med. Chem. Lett.* **2012**, *22*, 5625−5629.
(12) Estrada, A. a; Liu, X.; Baker-Glenn, C.; Beresford, A.; Burdick, D. J.; Chambers, M.; Chan, B. K.; Chen, H.; Ding, X.; DiPasquale, A. G.; Dominguez, S. L.; Dotson, J.; Drummond, J.; Flagella, M.; Flynn, S.; Fuji, R.; Gill, A.; Gunzner-Toste, J.; Harris, S. F.; Heffron, T. P.; Kleinheinz, T.; Lee, D. W.; Le Pichon, C. E.; Lyssikatos, J. P.; Medhurst, A. D.; Moffat, J. G.; Mukund, S.; Nash, K.; Scearce-Levie, K.; Sheng, Z.; Shore, D. G.; Tran, T.; Trivedi, N.; Wang, S.; Zhang, S.; Zhang, X.; Zhao, G.; Zhu, H.; Sweeney, Z. K. Discovery of Highly Potent, Selective, and Brain-Penetrable Leucine-Rich Repeat Kinase 2 (LRRK2) Small Molecule Inhibitors. *J. Med. Chem.* **2012**, *55*, 9416−9433.
(13) Chen, H.; Chan, B. K.; Drummond, J.; Estrada, A. a; Gunzner-Toste, J.; Liu, X.; Liu, Y.; Moffat, J.; Shore, D.; Sweeney, Z. K.; Tran, T.; Wang, S.; Zhao, G.; Zhu, H.; Burdick, D. J. Discovery of Selective LRRK2 Inhibitors Guided by Computational Analysis and Molecular Modeling. *J. Med. Chem.* **2012**, *55*, 5536−5545.
(14) Yun, H.; Heo, H. Y.; Kim, H. H.; Dookim, N.; Seol, W. Identification of Chemicals to Inhibit the Kinase Activity of Leucine-Rich Repeat Kinase 2 (LRRK2), a Parkinson's Disease-Associated Protein. *Bioorg. Med. Chem. Lett.* **2011**, *21*, 2953−2957.
(15) Ramsden, N.; Perrin, J.; Ren, Z.; Lee, B. D.; Zinn, N.; Dawson, V. L.; Tam, D.; Bova, M.; Lang, M.; Drewes, G.; Bantscheff, M.; Bard, F.; Dawson, T. M.; Hopf, C. Chemoproteomics-Based Design of Potent LRRK2-Selective Lead Compounds That Attenuate Parkinson's Disease-Related Toxicity in Human Neurons. *ACS Chem. Biol.* **2011**, 0−7.
(16) Fuji, R. N.; Flagella, M.; Baca, M.; Baptista, M. A. S.; Brodbeck, J.; Chan, B. K.; Fiske, B. K.; Honigberg, L.; Jubb, A. M.; Katavolos, P.; Lee, D. W.; Lin, T.; Liu, X.; Liu, S.; Lyssikatos, J. P.; Mahony, J. O.; Reichelt, M.; Roose-girma, M.; Sheng, Z.; Sherer, T.; Smith, A.; Solon, M.; Sweeney, Z. K.; Tarrant, J.; Urkowitz, A.; Warming, S.; Yaylaoglu, M.; Zhang, S.; Zhu, H.; Estrada, A. A.; Watts, R. J. Effect of Selective LRRK2 Kinase Inhibition on Nonhuman Primate Lung. *Sci. Transl. Med.* **2015**, *7*, 273ra15.
(17) Kramer, T.; Monte, F. Lo; Go, S.; Marlyse, G.; Amombo, O.; Schmidt, B. Small Molecule Kinase Inhibitors for LRRK2 and Their Application to Parkinson's Disease Models. *ACS Chem. Neurosci.* **2012**, *3*, 151−160.
(18) Ray, S.; Liu, M. Current Understanding of LRRK2 in Parkinson's Disease: Biochemical and Structural Features and Inhibitor Design. *Future Med. Chem.* **2012**, *4*, 1701−1713.
(19) Göring, S.; Taymans, J.-M.; Baekelandt, V.; Schmidt, B. Indolinone Based LRRK2 Kinase Inhibitors with a Key Hydrogen Bond. *Bioorg. Med. Chem. Lett.* **2014**, *24*, 4630−4637.
(20) Henderson, J. L.; Kormos, B. L.; Hayward, M. M.; Coffman, K. J.; Jasti, J.; Kurumbail, R. G.; Wager, T. T.; Verhoest, P. R.; Noell, G. S.; Chen, Y.; Needle, E.; Berger, Z.; Steyn, S. J.; Houle, C.; Hirst, W. D.; Galatsis, P. Discovery and Preclinical Profiling of 3-[4-(Morpholin-4-yl)-7*H*-pyrrolo[2,3-*d*]pyrimidin-5-yl]benzonitrile (PF-06447475), a Highly Potent, Selective, Brain Penetrant, and in Vivo Active LRRK2 Kinase Inhibitor. *J. Med. Chem.* **2015**, *58*, 419−432.
(21) Liu, Z.; Galemmo, R. a; Fraser, K. B.; Moehle, M. S.; Sen, S.; Volpicelli-Daley, L. A.; DeLucas, L. J.; Ross, L. J.; Valiyaveettil, J.; Moukha-Chafiq, O.; Pathak, A. K.; Ananthan, S.; Kezar, H.; White, E. L.; Gupta, V.; Maddry, J. A.; Suto, M. J.; West, A. B. Unique Functional and Structural Properties of the LRRK2 ATP-Binding Pocket. *J. Biol. Chem.* **2014**, *289*, 32937−32951.
(22) Gotthardt, K.; Weyand, M.; Kortholt, A.; Van Haastert, P. J. M.; Wittinghofer, A. Structure of the Roc-COR Domain Tandem of *C. tepidum*, a Prokaryotic Homologue of the Human LRRK2 Parkinson Kinase. *EMBO J.* **2008**, *27*, 2239−2249.
(23) Gilsbach, B. K.; Ho, F. Y.; Vetter, I. R.; van Haastert, P. J. M.; Wittinghofer, A.; Kortholt, A. Roco Kinase Structures Give Insights into the Mechanism of Parkinson Disease-Related Leucine-Rich-Repeat Kinase 2 Mutations. *Proc. Natl. Acad. Sci. U.S.A.* **2012**, *109*, 10322−10327.
(24) Zhang, J.; Yang, P. L.; Gray, N. S. Targeting Cancer with Small Molecule Kinase Inhibitors. *Nat. Rev. Cancer* **2009**, *9*, 28−39.
(25) Kornev, A. P.; Haste, N. M.; Taylor, S. S.; Eyck, L. F. Ten. Surface Comparison of Active and Inactive Protein Kinases Identifies a Conserved Activation Mechanism. *Proc. Natl. Acad. Sci. U.S.A.* **2006**, *103*, 17783−17788.
(26) Shenoy, A. R.; Visweswariah, S. S. Site-Directed Mutagenesis Using a Single Mutagenic Oligonucleotide and DpnI Digestion of Template DNA. *Anal. Biochem.* **2003**, *319*, 335−336.
(27) Mayer, M.; Meyer, B. Characterization of Ligand Binding by Saturation Transfer Difference NMR Spectroscopy. *Angew. Chem., Int. Ed.* **1999**, *38*, 1784−1788.
(28) Mayer, M.; Meyer, B. Group Epitope Mapping by Saturation Transfer Difference NMR to Identify Segments of a Ligand in Direct Contact with a Protein Receptor. *J. Am. Chem. Soc.* **2001**, *123*, 6108−6117.
(29) McCoy, M. A.; Senior, M. M.; Wyss, D. F. Screening of protein Kinases by ATP-STD NMR Spectroscopy. *J. Am. Chem. Soc.* **2005**, *127*, 7978−7979.
(30) Blanc, J.; Geney, R.; Menet, C. Type II Kinase Inhibitors: An Opportunity in Cancer Rational Design. *Anti-Cancer Agents Med. Chem.* **2013**, *13*, 1−17.

DOI: 10.1021/jm5018779
J. Med. Chem. 2015, 58, 3751−3756